ARTICLES
PUBLISHED ONLINE: 26 JUNE 2011 | DOI: 10.1038/NGEO1184

nature geoscience

Loading of the San Andreas fault by flood-induced rupture of faults beneath the Salton Sea

Daniel Brothers[1]*, Debi Kilb[2], Karen Luttrell[2†], Neal Driscoll[2] and Graham Kent[3]

The southern San Andreas fault has not experienced a large earthquake for approximately 300 years, yet the previous five earthquakes occurred at ∼180-year intervals. Large strike-slip faults are often segmented by lateral stepover zones. Movement on smaller faults within a stepover zone could perturb the main fault segments and potentially trigger a large earthquake. The southern San Andreas fault terminates in an extensional stepover zone beneath the Salton Sea—a lake that has experienced periodic flooding and desiccation since the late Holocene. Here we reconstruct the magnitude and timing of fault activity beneath the Salton Sea over several earthquake cycles. We observe coincident timing between flooding events, stepover fault displacement and ruptures on the San Andreas fault. Using Coulomb stress models, we show that the combined effect of lake loading, stepover fault movement and increased pore pressure could increase stress on the southern San Andreas fault to levels sufficient to induce failure. We conclude that rupture of the stepover faults, caused by periodic flooding of the palaeo-Salton Sea and by tectonic forcing, had the potential to trigger earthquake rupture on the southern San Andreas fault. Extensional stepover zones are highly susceptible to rapid stress loading and thus the Salton Sea may be a nucleation point for large ruptures on the southern San Andreas fault.

Fault stepover zones are prone to transient stress perturbations and may play an important role in earthquake initiation[1]. Few geologic records have documented the relationship between stress-loading events in a stepover zone and ruptures on the bounding strike-slip faults; most studies are based on field mapping and numerical modelling of historical fault ruptures[2,3]. Processes involving transient pore pressure changes (for example, from lake filling; ref. 4) and static stress loading from fault displacement[5] have been associated with earthquake triggering and increased seismicity. Lake loading and fault movement in the Salton Sea transtensional stepover zone[6] can create stress perturbations that may have the potential to trigger earthquakes on the southern San Andreas fault (SSAF).

Tectonics and flooding of the Salton Sea region

The Salton Trough is isolated from the Gulf of California by the subaerial Colorado River delta[7]. Episodic, late-Holocene diversions of the Colorado River into the Salton Trough flooded the basin to ∼13 m above sea level (the elevation of the topographic sill; Fig. 1) forming ancient Lake Cahuilla[7,8] (LC), which had an area greater than 5,700 km^2 and a maximum depth of ∼100 m. The most robust palaeoseismic history on the SSAF is recorded in sediment deposited during transgressive and regressive cycles of LC (ref. 9). At present the Salton Sea covers the depocenter of LC sediments where records of lake flooding/desiccation cycles are preserved in a rapidly subsiding stepover basin that separates two right-lateral fault systems: the SSAF and the Imperial fault[6] (Fig. 1).

Several active growth faults exhibiting large components of extension were recently discovered beneath the Salton Sea, near the southern terminus of the SSAF (ref. 6; Fig. 1 and Supplementary Fig. S1); many seem to be kinematically linked to the SSAF. These faults trend ∼N15° E, exhibit down-to-the-southeast displacement

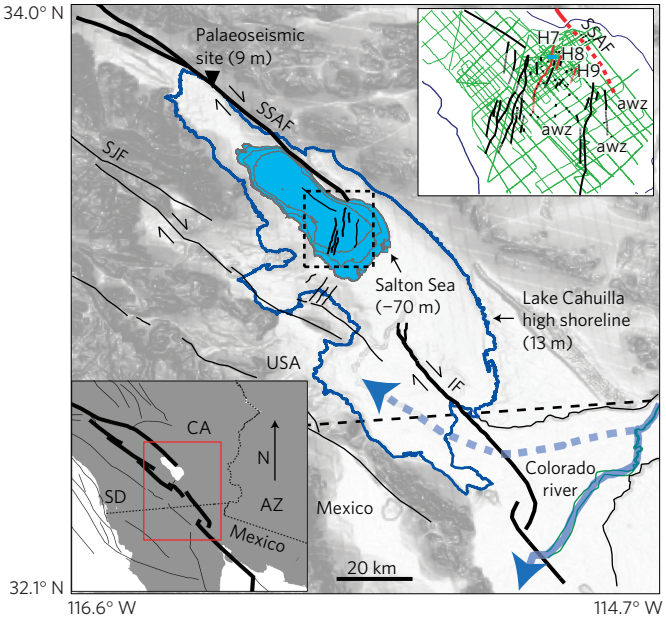

Figure 1 | Geologic setting of the study region. Active faults are shown as black lines, including the SSAF, San Jacinto fault (SJF), Imperial fault (IF) and a series of N15 ° E trending extensional faults in the Salton Sea[6]. The inverted triangle marks the Coachella palaeoseismic site[9]; the dashed box represents the area of the top inset. Colorado River normal (blue arrow) and diversion (dashed arrow) flow paths. Top inset: Seismic reflection profiles (green lines), faults analysed in detail (H7, H8, H9—red lines), and acoustic wipeout zones (awz). The blue bar marks the location of Figs 2 and 3. Bottom inset: Regional map showing location of the study.

[1]Woods Hole Coastal and Marine Science Center, US Geological Survey, 384 Woods Hole Road, Woods Hole, Massachusetts 02543, USA, [2]Scripps Institution of Oceanography, University of California, San Diego, 9500 Gilman Drive, La Jolla, California 92093, USA, [3]Nevada Seismological Laboratory, University of Nevada, Reno, MS-174, Reno, Neveda 89557, USA. †Present address: US Geological Survey, 345 Middlefield Road, Menlo Park, California 94025, USA. *e-mail: dbrothers@usgs.gov.

© 2011 Macmillan Publishers Limited. All rights reserved.

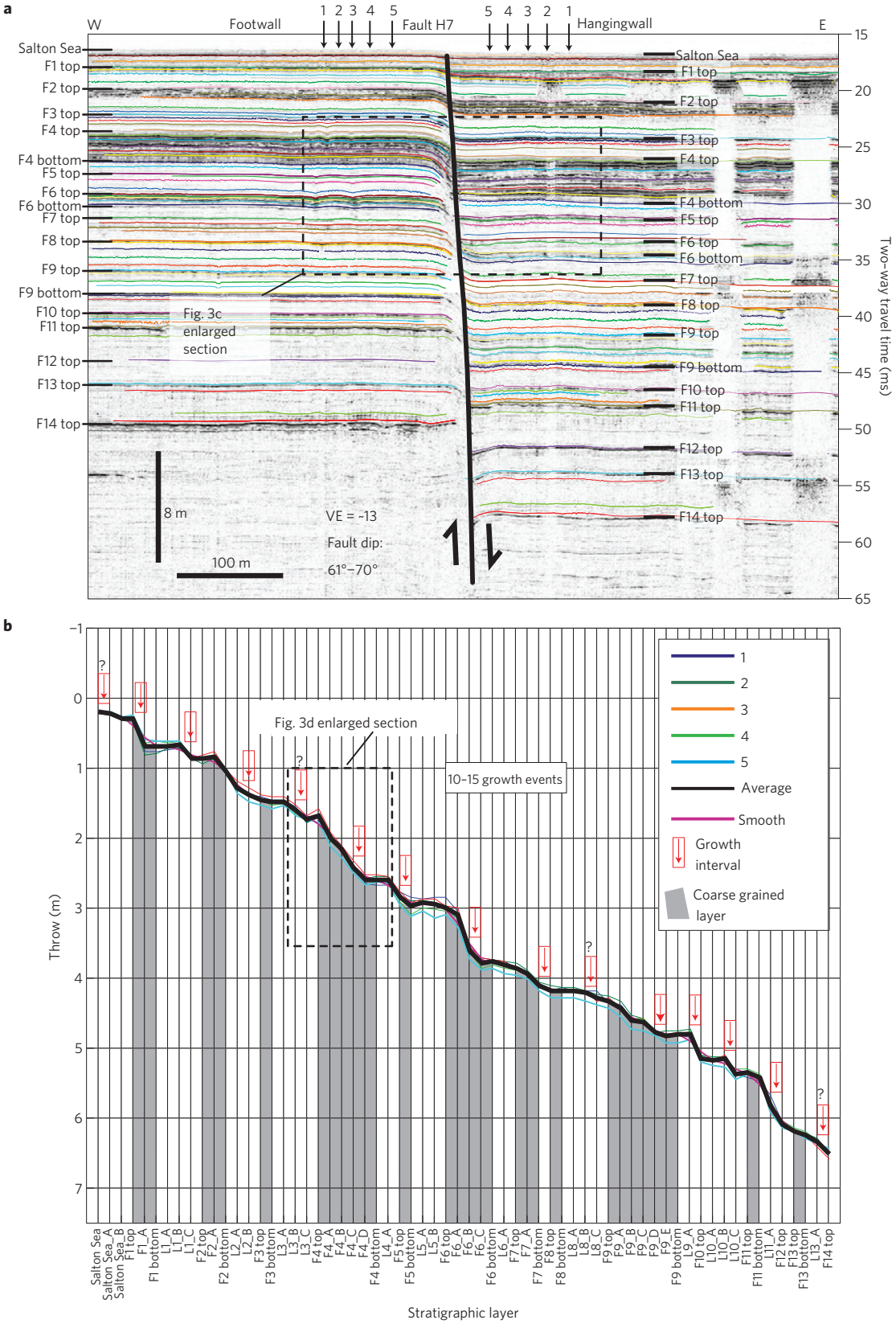

Figure 2 | Interpreted seismic CHIRP profile (see Fig. 1 for location). a, Digitized acoustic horizons used to measure fault throw. Coarse-grained, high-amplitude (flood) packages (F) and fine-grained low-amplitude lacustrine packages (L) are labelled on both the hangingwall and footwall. Fault throw was measured across each horizon along five separate profiles that are distributed at ~20 m increments on the footwall and hangingwall (numerically labelled arrows at top of image). **b**, Throw by stratigraphic layer. Some growth events, marked by '?', may represent residual throw from an earlier event that is infilled by subsequent deposition. Numbered profiles correspond to measurement locations (vertical arrows) shown above in **a**.

© 2011 Macmillan Publishers Limited. All rights reserved.

NATURE GEOSCIENCE DOI: 10.1038/NGEO1184

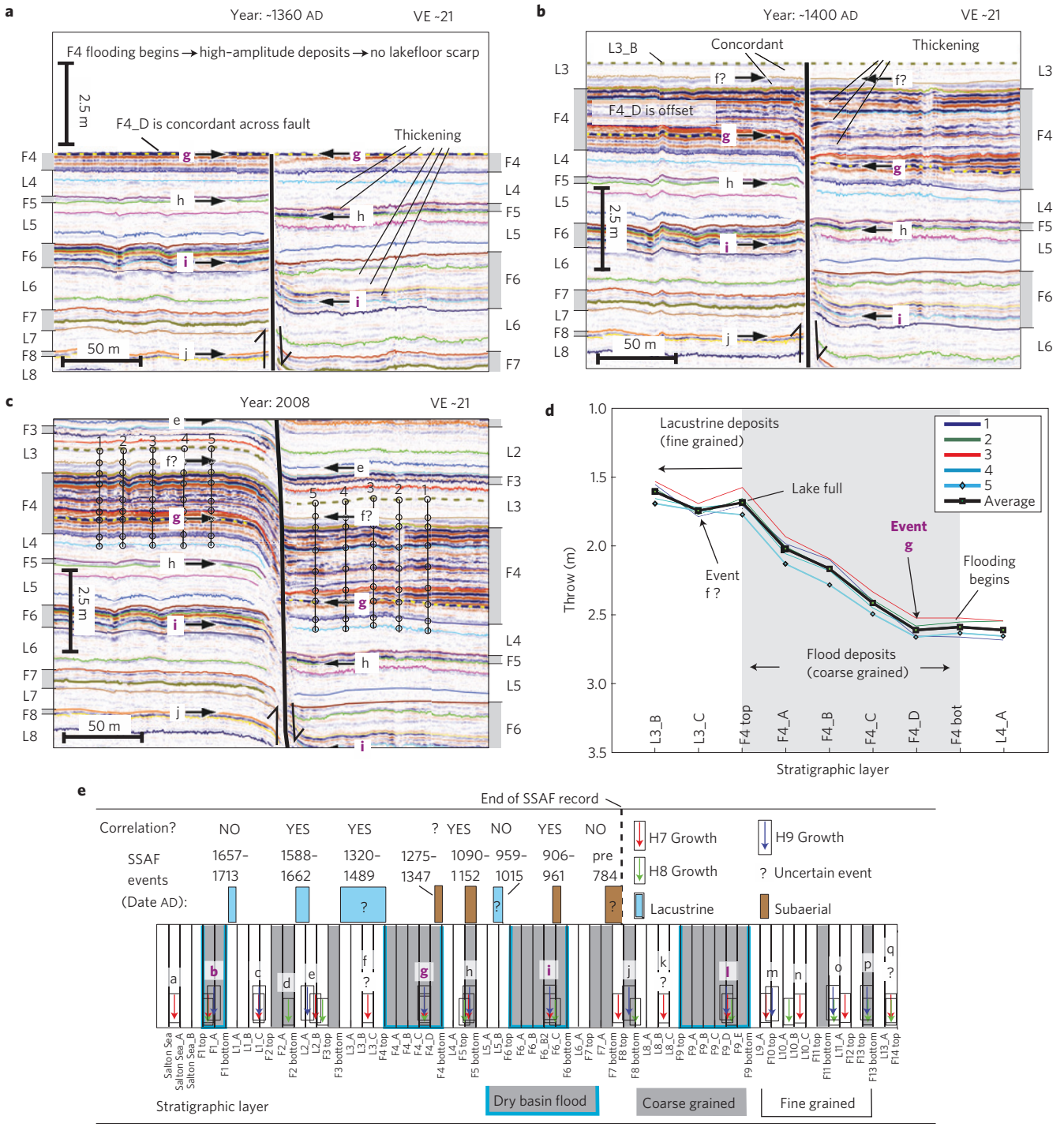

Figure 3 | Example of fault displacement during LC flooding. Acoustic amplitudes are used to differentiate high-stand lake deposits ('L') from flood deposits ('F'). Lower-case letters indicate displacement events; bold, purple letters are displacements during flooding. **a**, Flattened section showing concordant stratigraphy during the early stage of flooding (pre-earthquake). **b**, Displacement across horizon 'g' with subsequent thickening on the hangingwall and onlap onto the footwall. **c**, Present-day stratigraphy (cumulative fault growth). Vertically aligned circles represent throw measurements in **d**. **d**, Quantitative evidence that event 'g' occurred during flooding. **e**, Summary of fault growth for faults H7, H8 and H9; SSAF palaeoearthqaukes[9] are superimposed.

and have vertical slip-rates between 1 and 4 mm yr^{-1}. Depositional transitions from fan delta to deep-water lacustrine facies beneath the Salton Sea record lake-filling episodes of the basin. Lithological and grain-size measurements from cone penetration tests and offshore borings[10] were used to ground truth seismic CHIRP profiles. Transgressive and regressive surfaces identified offshore in seismic stratigraphy[6] were correlated with stratigraphy at a palaeoseismic site to the north of the Salton Sea[9]. Here, we extract the magnitude and timing of fault activity over several earthquake cycles from sedimentary records beneath the Salton Sea. We then use this information to study relationships between SSAF earthquakes, fault displacements in the stepover zone, and pervasive

© 2011 Macmillan Publishers Limited. All rights reserved.

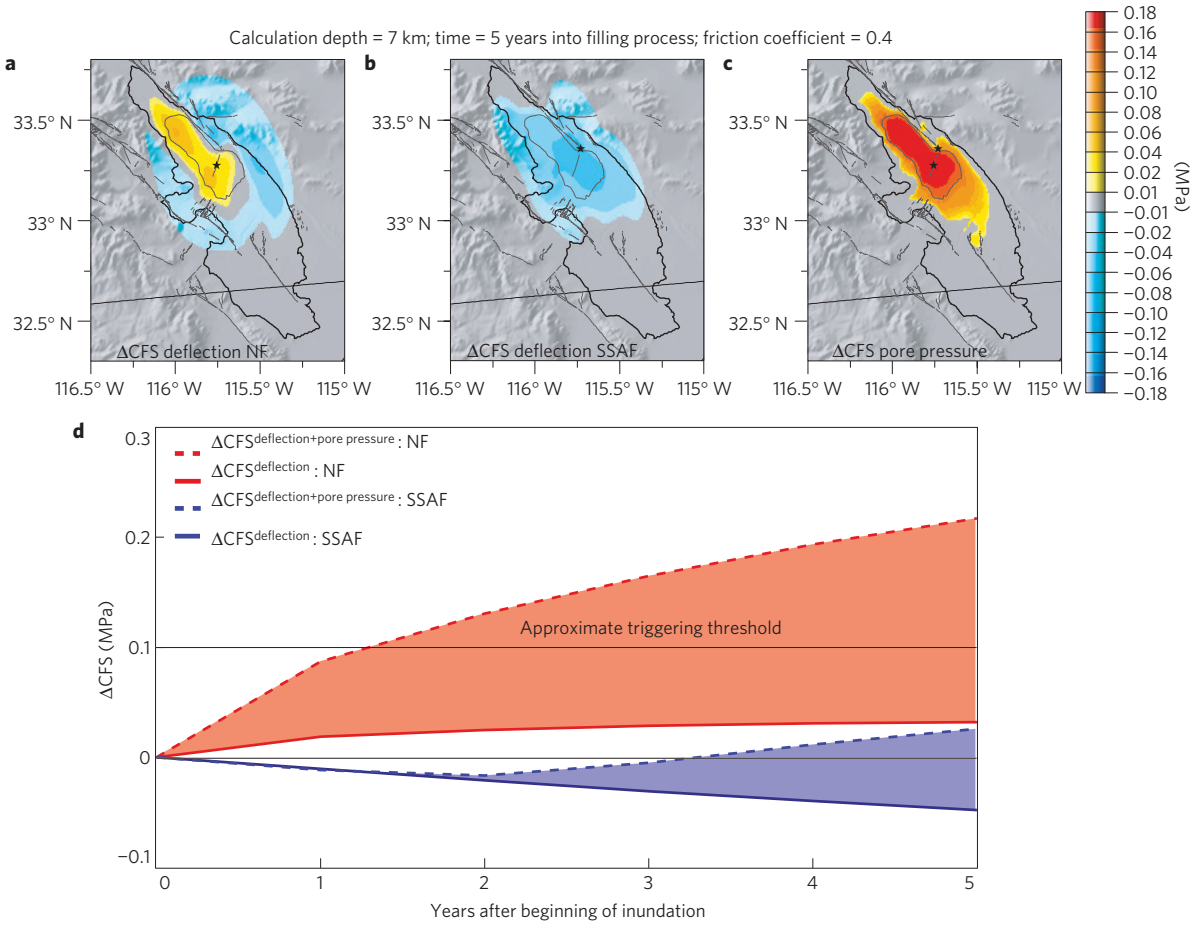

Figure 4 | Coulomb stress map (ΔCFS) from LC inundation. a, Loading from mechanical bending resolved onto normal fault (NF) planes striking N15 ° E and dipping 65° SE; and **b**, resolved on SSAF-type vertical dextral strike-slip planes striking N35° W. Black line represents high-shoreline. **c**, ΔCFS from hydrostatic pore pressure changes based on the depth of the lake (maximum end member). **d**, Range of possible ΔCFS during first five years of lake filling on the NF and the SSAF (exact position indicated by the stars in **a**–**c**).

flooding. We propose that loading by LC may have induced failure on faults beneath the Salton Sea that, in turn, had the potential to trigger an earthquake rupture on the SSAF.

Fault displacement history and stress modelling

Detailed seismic CHIRP surveys were conducted in the Salton Sea between 2006 and 2009 (ref. 6; Fig. 1). Acoustic horizons represent depositional events that were subsequently buried. In the southern Salton Sea, sediment accumulation averaged over the last ~1,200 years is nearly 2 cm yr^{-1}, therefore the 1–15 kHz swept CHIRP pulse can provide decadal-scale stratigraphic resolution. During flooding episodes, sedimentation rates can be as high as 50 cm yr^{-1} in the southern Salton Sea, yielding annually resolvable depositional records. Variations in stratal geometry, acoustic character and lithology represent cycling between rapidly deposited Colorado River flood deposits, high-stand lacustrine deposits and, in some areas, thin, reworked subaerial deposits. Evidence for subaerial exposure and fluvial incision suggests that complete desiccation of LC occurred only four times during the last few thousand years (layers F1, F4, F6 and F9 in Fig. 2a; Supplementary Figs S2 and S3). When the Colorado River flooded into a dry basin, a thick wedge of coarse-grained delta and fan delta material was deposited above an exposure surface, with the maximum thickness in the southern Salton Sea. At other times, relatively thin flood deposits mark the boundaries of most sequences, meaning shoreline regression was brief and the Colorado River probably spilled into an existing lake.

We reconstructed the timing of fault displacement using quantitative analyses of vertical throw (assuming a p wave velocity of 1,600 m s^{-1}) along more than 65 acoustic horizons that are offset by three of the most active extensional faults in the Salton Sea (Fig. 2; Supplementary Figs S2 and S3). We plot the throw across each horizon to examine the interplay between fault displacement and sedimentary dynamics[11,12]. In a simple model, negative slopes on the throw-plots, or abrupt increases in throw, indicate periods of fault activity and subsequent infill. Intervals without thickening and/or periods of fault quiescence are observed as null slopes, and positive slopes may indicate fault inversion or erosion of the footwall. As sedimentation rates outpace fault displacement rates (note the absence of surface scarps), we assume that hangingwall accommodation is rapidly infilled and abrupt slope changes in the throw plots represent individual displacement events. High-stand (fine-grained) and low-stand (coarse-grained) deposits show discrete intervals of thickening from the footwall to the hangingwall. The low-stand deposits in the southern Salton Sea are predominantly Colorado River fan delta facies that preferentially infill the hangingwall accommodation.

Throw plots reveal at least eight events on each of the three most active faults imaged near the SSAF, and several events seem coincident amongst these faults. Vertical displacement per event varies between 0.2 and 1.0 m and is punctuated, occurring over short time intervals. Such a sawtooth pattern suggests that steady background creep is not a significant contributor to throw accumulation. We digitally flattened horizons to identify changes

© 2011 Macmillan Publishers Limited. All rights reserved.

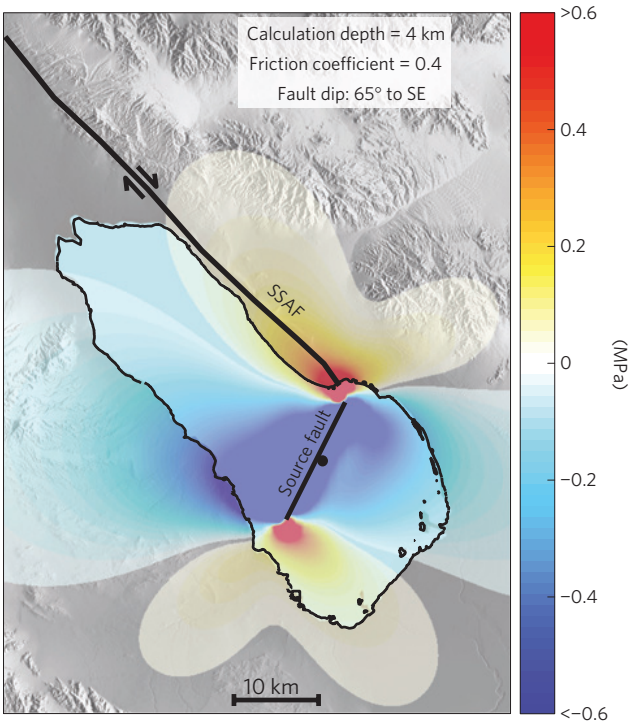

Figure 5 | Coulomb stress (ΔCFS) generated by rupture of a normal fault beneath the Salton Sea. The simulation applies 1.0 m of normal displacement to the source fault. Resulting stresses are derived on fault planes oriented similar to the SSAF (strike = 325°; dip = 90°; rake = 180°). Warm colours indicate areas where failure is promoted and cool colours where failure is inhibited. Stress lobes are saturated at ±0.6 MPa.

in stratal geometry due to fault displacement (Fig. 3a–c) and on all three faults, displacement growth and hangingwall onlap are observed during Colorado River flooding. The basal subunits for some flooding layers (F1, F4, F6 and F9) are concordant across the fault; that is, no surface scarp existed at the onset of flooding (Fig. 3a,d). Subsequent displacement-generated accommodation was mostly infilled by high-amplitude sediment during flooding and preceded the deposition of fine-grained (low-amplitude) highstand facies (Fig. 3b–d). Comparable timing between flooding and fault growth is observed on three separate faults (Fig. 3e) during four separate flood intervals. Comparison between offshore fault displacement and SSAF earthquakes[9] is based solely on the relative stratigraphic position of events (see Methods). Of the five most probable SSAF events determined from palaeoseismic records[9], at least three may have been coincident with displacement on offshore faults and of the eight potential SSAF palaeoearthquakes, at least four overlap with offshore displacement (Fig. 3e). Based on these records, at least one of the last three dry-basin floods coincides with an earthquake on the SSAF.

To investigate the effects of LC flooding on faults, we estimate static Coulomb failure stress changes (ΔCFS) induced by an added load of the lake water and increased pore pressure[5,13]. We assume a constant lake filling rate during floods, in which the high-shoreline (13 m) is reached in 20 years[8], and model how two different fault systems respond to lake-filling. The first resolves stresses on normal faults striking N15° E and dipping 65° SE (Fig. 1), as observed in the seismic CHIRP profiles, and the second resolves stresses on vertical dextral faults striking N35° W, similar to the SSAF (Fig. 4). Faults are assumed to be simple planar features that extend to 7 km depth, which is the mean depth of seismicity in and around the Salton Sea[14,15]. Although constraints on fault geometry at depth are limited, dramatic changes in dip (for example, listric faulting) are not observed in the upper kilometre[16], and the fault geometry we use in our models is consistent with analogue models for young pull-apart basins[6]. Results show that during the first five years of lake filling, deformation induced by plate bending in the lake region increases ΔCFS on the normal faults by 0.03 MPa and decreases it by 0.05 MPa on the SSAF. These stresses are not by themselves enough to either trigger or obstruct a rupture on either fault (the expected threshold for triggering is ∼0.1 MPa; ref. 5). However, if we assume the maximum effect for pore pressure, where pore fluids permeate hydrostatically to seismogenic depths, ΔCFS increases by an additional 0.18 MPa on the normal faults and 0.08 MPa on the SSAF. As lake filling continues, the additive effects of plate bending and pore pressure will increase ΔCFS up to 0.4 MPa on the normal faults and 0.13 MPa on the SSAF (Supplementary Movie S4). After lake filling ceases, ΔCFS on both faults will decay as viscous rebound processes relax the asthenosphere in response to the new load.

We next investigate the causal relationship between displacement on normal faults in the Salton Sea and SSAF earthquakes. Although we cannot ascertain the total seismic moment or precise mechanism of fault displacement, the seismic stratigraphy has sufficient temporal resolution to show that growth occurs over short time periods relative to lithospheric viscoelastic relaxation time. Both seismic and punctuated aseismic displacement would generate static stress changes. Using an elastic half-space model[17–19], we estimate static stress changes from a 1.0 m normal displacement, equivalent to a magnitude 6 earthquake, on one of the extensional faults in the Salton Sea. The resulting ΔCFS field (Fig. 5) has a northwest oriented lobe of positive ΔCFS along the trend of the SSAF, including a 1.1–1.4 MPa increase where the SSAF intersects the shoreline. The ΔCFS along the SSAF may be significantly higher than modelled if the two fault systems are directly connected.

Flood-induced fault rupture

Both observation and modelling suggest that capture of the Colorado River flooding into a dry basin provides optimal conditions for triggered rupture on normal faults beneath the lake and subsequent triggering on the SSAF. The additive ΔCFS from lake flooding (up to 0.13 MPa) and normal fault displacement (up to 1.4 MPa) are sufficiently high to trigger an earthquake on the SSAF, particularly if lake filling triggers simultaneous rupture of several normal faults, as the stratigraphic records suggest. Historical data partially supports this apparent causality. Layer F1 shows evidence for fault growth (Figs 2b and 3e) during flooding of today's Salton Sea (1905–1907). The timing of the flooding is consistent with a M 6.1 event located near the southern Salton Sea, which may have been triggered by combined effects from lake loading and static/dynamic stresses from the 1906 San Francisco earthquake[20].

There are two sources of uncertainty in our approach that need to be addressed. First, pore pressure at seismogenic depths is expected to be highly variable based on the complex structural and magmatic framework of the basin[6,21,22]. Impermeable sediment layers (for example, Brawley formation; ref. 23) may prevent vertical downward migration of pore fluids during lake flooding. But the compressive weight of the water column above an aquitard could cause transient elevated pore pressure in layers below, and faults and fractures may also allow for pore fluid exchange at depth. Exploratory wells[24,25] ∼12 km to the south of the normal faults indicate hydrothermal reservoirs (potential zones of overpressure) are actually near hydrostatic equilibrium. Although speculative, if overpressures across the normal faults did exist, clamping stresses would be lowered, potentially allowing load-induced bending stresses to trigger displacement on the normal faults. If pore pressure increases by only a fraction of the hydrostatic load during LC flooding, ΔCFS on normal faults would exceed the assumed 0.1 MPa triggering threshold. Second, large ruptures along the SSAF

© 2011 Macmillan Publishers Limited. All rights reserved.

may have promoted failure of the normal faults; however, existing geologic records cannot resolve which fault system ruptured first. Regardless, the relative frequency of dip-slip fault displacements, coincident timing between displacements and palaeoearthquakes on the SSAF, and high levels of persistent microseismicity and earthquake swarms beneath the Salton Sea[15,26] all suggest the Salton Sea region is a potential nucleation point for future ruptures on the SSAF.

A palaeoseismic study near the LC high shoreline (9 m elevation; Fig. 1) argued against concurrent LC flooding and SSAF earthquakes[9] and also proposed that liquefaction of Colorado River channel banks during SSAF earthquakes may be the primary cause for Colorado River diversions into the basin. Because of its location at the high shoreline, the stratigraphic record of LC at the palaeoseismic site is incomplete. As a result of fluctuations in the LC shoreline, depositional records near the high-water mark are not ideal for examining the relative timing between lake flooding and earthquakes. For example, the thick (>1 m) Colorado River fan-delta packages that allow us to decipher the relative timing between fault displacement and LC filling are not documented outside the present-day Salton Sea[8,9,27]. Extreme flooding within the Colorado River watershed associated with short- and long-term regional climate patterns offers another plausible mechanism for river avulsion and flooding of the basin. Reduced flood frequency in the watershed between 1200 and 1400 AD corresponds to a prolonged period of LC low-stand, and increased flooding before and after 1200–1400 AD coincides with several LC highstands[9,28]. Nevertheless, the important results from the palaeoseismic study[9] and the findings reported here allow for detailed comparisons between records of fault displacement and lake flooding in the basin depocenter and palaeoseismic events on the SSAF.

Earthquake hazard concerns

Based on the ~180 year average recurrence for palaeoearthquakes on the SSAF (ref. 9) and evidence that this fault has continued to accumulate large amounts of strain since the most recent large earthquake in ~1700 AD (refs 29,30), it is commonly believed that the SSAF is ~100 years 'overdue' for a large earthquake[31]. In addition to possible changes in background driving stress[32], the absence of rapid stress loading induced by LC floods may have also contributed to the prolonged interseismic period. As anthropogenic control of the Colorado River makes future inundation of the Salton Trough highly unlikely, our present concern is the potential for rupture of extensional faults within the Salton Sea stepover zone, independent of flooding, to trigger a large earthquake on the SSAF. Strike-slip stepover zones often act as segment boundaries that define barriers during rupture propagation[3], but they also have the potential to act as nucleation points for large earthquakes[1]. Much like the M 7.9 1906 San Francisco earthquake is believed to have nucleated in a strike-slip stepover[33], the Salton Sea stepover is a possible nucleation point for a future SSAF rupture. Such an event could propagate northward, producing strong shaking and significant damage to the Los Angeles metropolitan area[34].

Methods

We employed a number of criteria to determine if the events observed on the cross faults in the Salton Sea and at the palaeoseismic site (9 m elevation; Fig. 1) are correlative. First and foremost, did the events occur within the same lake sequence at both sites? At the palaeoseismic site in Fig. 3e, SSAF earthquakes that occur during LC highstand are shaded blue and ones that occur during subaerial conditions are shaded brown. To further facilitate the correlation, the lake stands are labelled on the bottom of Fig. 3e. When an event is recorded in different depositional environments, one subaerial (palaeoseismic site) and one lacustrine (Salton Sea), shoreline position and fluctuations were taken into account. The correlation was marked 'YES' when events occurred in the same layer, events marked '?' occur in different layers, but could be temporally coincident if the shoreline was somewhere between highstand and lowstand positions, and events marked 'NO' seem outside the range of possibilities. Note b, g, i, and l events occur when the Colorado River is flooding a dry basin (F1, F4, F6 and F9). Conversely, d, h, j and p events occur when the Colorado River flows into an existing lake.

Stress from increasing pore pressure is calculated as $\Delta CFS^{porepressure} = \mu' \rho_w g h$, where ρ_w is the water density, g is the acceleration of gravity, h is the lake water depth, and μ' is the effective fault friction coefficient. This is the hydrostatic endmember, that is independent of fault orientation and presumes pore fluids permeate hydrostatically to seismogenic depth, and should therefore be considered a maximum. Stresses induced by mechanical deformation in response to the weight of the lake water are computed as an elastic plate overlying a Maxwell viscoelastic halfspace[13]. Model parameters assume a 35 km thick plate and a halfspace relaxation period of 30 years (corresponding to a viscosity of 1.3×10^{19} Pa s). As we are principally focused on the short timescale of lake filling, our results are insensitive to elastic thickness as this parameter only affects the shape of viscous rebound. Stresses are computed at 7 km depth, which is the median seismogenic depth for this region[14]. We use a coefficient of friction of 0.4, which is an intermediate value for the region[5]. The ΔCFS shown in Fig. 4 ranges from the minimum stress affected by mechanical deformation only to the maximum stress affected by both mechanical deformation and full hydrostatic pore pressure at seismogenic depth. Note a previous LC modelling study[13] included a code error that tended to overestimate the elastic response of the SSAF to lake loading. The error was subsequently corrected[35] and model results presented here are correct and supersede those of the previous study.

We model static Coulomb stress changes (ΔCFS) induced by fault displacement using the Coulomb-3 software code[17–19]. The calculations require input geometry and displacement on the faults that impart stresses (sources) and faults on which the stresses are imparted (receivers). Source fault parameters were constrained by the strike, dip and displacement per event measurements from seismic reflection profiles. We applied a 1.0 m normal displacement based on vertical throw measurements. Figure 5 used a friction coefficient of 0.4 and was calculated at a depth of 4 km on a 65° SE dipping, 15 km long, 8 km deep fault plane. We expect a small component of sinistral slip (not modelled) on the offshore faults based on seismicity patterns[15], earthquake source mechanisms[36] and evidence for strike-slip deformation in the CHIRP imagery (for example, Supplementary Fig. S3), which would further increase the Coulomb stress on the SSAF.

We completed a suite of parameter sensitivity tests for both the lake loading and earthquake rupture models that addressed variations in the frictional coefficients, elastic plate thickness, depth of observation, and rupture fault location. For our purposes, these sensitivity tests indicate minimal variations in the spatial distributions of stress and their magnitudes. As stated, elastic thickness has little to no effect on the immediate (elastic) response to lake loading. The largest variations depend on the coefficient of friction (Supplementary Fig. S5). The effect of changes in friction on ΔCFS from earthquake rupture is small because its primary contribution is from changes in shear stress. The effect on ΔCFS from lake loading is larger because it is dominated by contributions from normal stress. Overall, the models presented in this study represent conservative selections and the conclusions are robust to model parameter choices.

Received 19 November 2010; accepted 17 May 2011; published online 26 June 2011

References

1. King, G. & Nabelek, J. Role of fault bends in the initiation and termination of earthquake rupture. *Science* **228,** 984–987 (1985).
2. Oglesby, D. D. The dynamics of strike-slip step-overs with linking dip-slip faults. *Bull. Seismol. Soc. Am.* **95,** 1604–1622 (2005).
3. Wesnousky, S. G. Predicting the endpoints of earthquake ruptures. *Nature* **444,** 358–360 (2006).
4. Simpson, D. W., Leith, W. S. & Scholz, C. H. 2 types of reservoir-induced seismicity. *Bull. Seismol. Soc. Am.* **78,** 2025–2040 (1988).
5. King, G. C. P., Stein, R. S. & Lin, J. Static stress changes and the triggering of earthquakes. *Bull. Seismol. Soc. Am.* **84,** 935–953 (1994).
6. Brothers, D. S. *et al.* Tectonic evolution of the Salton Sea inferred from seismic reflection data. *Nature Geosci.* **2,** 581–584 (2009).
7. Van De Kamp, P. C. Holocene continental sedimentation in Salton-Basin, California—Reconnaissance. *Geol. Soc. Am. Bull.* **84,** 827–848 (1973).
8. Waters, M. R. Late holocene lacustrine chronology and archaeology of ancient Lake Cahuilla, California. *Quat. Res.* **19,** 373–387 (1983).
9. Philibosian, B., Fumal, T. E. & Weldon, R. San Andreas Fault earthquake chronology and Lake Cahuilla history at Coachella, California. *Bull. Seismol. Soc. Am.* **101,** 13–38 (2011).
10. URS. Preliminary in-sea geotechnical investigation, Salton Sea Resoration Project Report, Riverside and Imperial Counties, California. 399 (2004).
11. Cartwright, J., Bouroullec, R., James, D. & Johnson, H. Polycyclic motion history of some Gulf Coast growth faults from high-resolution displacement analysis. *Geology* **26,** 819–822 (1998).
12. Castelltort, S., Pochat, S. & Van den Driessche, J. J. Using T–Z plots as a graphical method to infer lithological variations from growth strata. *J. Struct. Geol.* **26,** 1425–1432 (2004).

© 2011 Macmillan Publishers Limited. All rights reserved.

13. Luttrell, K., Sandwell, D., Smith-Konter, B., Bills, B. & Bock, Y. Modulation of the earthquake cycle at the southern San Andreas fault by lake loading. *J. Geophys. Res.* **112,** B08411 (2007).
14. Nazareth, J. J. & Hauksson, E. The seismogenic thickness of the southern California crust. *Bull. Seismol. Soc. Am.* **94,** 940–960 (2004).
15. Lin, G. Q., Shearer, P. M. & Hauksson, E. Applying a three-dimensional velocity model, waveform cross correlation, and cluster analysis to locate southern California seismicity from 1981 to 2005. *J. Geophys. Res.* **112,** B12309 (2007).
16. Kell-Hills, A. M., Kent, G. M., Driscoll, N. W., Harding, A. J. & Baskin, R. L. Seismic reflection study of the Salton Sea. *SCEC Ann. Mtg. Proc. Abstr.* **XX,** 181–181 (2010).
17. Toda, S., Stein, R. S., Richards-Dinger, K. & Bozkurt, S. B. Forecasting the evolution of seismicity in southern California: Animations built on earthquake stress transfer. *J. Geophys. Res.* **110,** B05S16 (2005).
18. Okada, Y. Internal deformation due to shear and tensile faults in a half-space. *Bull. Seismol. Soc. Am.* **82,** 1018–1040 (1992).
19. Lin, J. & Stein, R. S. Stress triggering in thrust and subduction earthquakes and stress interaction between the southern San Andreas and nearby thrust and strike-slip faults. *J. Geophys. Res.-Solid Earth* **109,** B02303 (2004).
20. Meltzner, A. J. & Wald, D. J. Aftershocks and triggered events of the Great 1906 California earthquake. *Bull. Seismol. Soc. Am.* **93,** 2160–2186 (2003).
21. Fuis, G. S., Mooney, W. D., Healy, J. H., Mcmechan, G. A. & Lutter, W. J. A Seismic Refraction Survey of the Imperial-Valley region, California. *J. Geophys. Res.* **89,** 1165–1189 (1984).
22. Schmitt, A. K. & Vazquez, J. A. Alteration and remelting of nascent oceanic crust during continental rupture: Evidence from zircon geochemistry of rhyolites and xenoliths from the Salton Trough, California. *Earth Planet. Sci. Lett.* **252,** 260–274 (2006).
23. Dibblee, T. W. Geology of the Imperial Valley Regioin, Californa. *Cali. Bur. Mines Bull.* **170,** 21–28 (1954).
24. Helgeson, H. C. Geologic and thermodynamic characteristics of Salton Sea geothermal system. *Am. J. Sci.* **266,** 129–166 (1968).
25. Newmark, R. L., Kasameyer, P. W. & Younker, L. W. Shallow drilling in the Salton-Sea region—the thermal anomaly. *J. Geophys. Res.* **93,** 13005–13023 (1988).
26. Kilb, D. *State of Stress at the Southernmost End of the San Andreas Fault: Integration of Seismicity Patterns and Focal Mechanisms with Fault Structure Observed in Seismic Reflection Data Beneath the Salton Sea*. USGS NEHRP Final Technical Report (2009).
27. Meltzner, A. J., Rockwell, T. K. & Owen, L. A. Recent and long-term behavior of the Brawley fault zone, Imperial Valley, California: An escalation in slip rate? *Bull. Seismol. Soc. Am.* **96,** 2304–2328 (2006).
28. Ely, L. L. Response of extreme floods in the southwestern United States to climatic variations in the late Holocene. *Geomorphology* **19,** 175–201 (1997).
29. Sieh, K. E. & Williams, P. L. Behavior of the Southernmost San-Andreas Fault during the Past 300 Years. *J. Geophys. Res.* **95,** 6629–6645 (1990).
30. Fialko, Y. Interseismic strain accumulation and the earthquake potential on the southern San Andreas fault system. *Nature* **441,** 968–971 (2006).
31. Field, E. H. *et al.* Uniform California Earthquake Rupture Forecast, Version 2 (UCERF 2). *Bull. Seismol. Soc. Am.* **99,** 2053–2107 (2009).
32. Dieterich, J. A constitutive law for rate of earthquake production and its application to earthquake clustering. *J. Geophys. Res.* **99,** 2601–2618 (1994).
33. Zoback, M. L., Jachens, R. C. & Olson, J. A. Abrupt along-strike change in tectonic style: San Andreas fault zone, San Francisco Peninsula. *J. Geophys. Res.* **104,** 10719–10742 (1999).
34. Olsen, K. B. *et al.* Strong shaking in Los Angeles expected from southern San Andreas earthquake. *Geophys. Res. Lett.* **33,** L07305 (2006).
35. Luttrell, K. & Sandwell, D. Ocean loading effects on stress at near shore plate boundary fault systems. *J. Geophys. Res.* **115,** B08411 (2010).
36. Hardebeck, J. L. & Shearer, P. M. Using S/P amplitude ratios to constrain the focal mechanisms of small earthquakes. *Bull. Seismol. Soc. Am.* **93,** 2434–2444 (2003).

Acknowledgements

The California Department of Water Resources, the California Department of Fish and Game, and the Scripps Institution of Oceanography funded the geophysical surveys in the Salton Sea. D.B., N.D. and G.K. were also supported by the National Science Foundation (Division of Ocean Sciences) and the Southern California Earthquake Center. Work by D.B. and D.K. was funded by a USGS NEHRP grant. K.L. was supported by the NASA Earth and Space Science Fellowship Program and the National Science Foundation (Division of Ocean Sciences). We thank U. ten Brink, D. Sandwell, D. Kane, and M. Curan for helpful reviews.

Author contributions

D.B. and D.K. collaboratively oversaw this project, outlined the proposed work and prepared the majority of the manuscript. D.B., N.D. and G.K. and were responsible for seismic reflection data collection and geologic interpretation. D.B., D.K. and K.L. were responsible for the stress modelling. All authors contributed to the final manuscript.

Additional information

The authors declare no competing financial interests. Supplementary information accompanies this paper on www.nature.com/naturegeoscience. Reprints and permissions information is available online at http://www.nature.com/reprints. Correspondence and requests for materials should be addressed to D.B.

© 2011 Macmillan Publishers Limited. All rights reserved.